TECHNICAL PAPER

MR89-143

Theoretical Analysis of Frictional Effect on Circular Brush Stiffness Properties

authors

C. Y. SHIA
Graduate Research Assistant
Marquette University
Milwaukee, Wisconsin

R. J. STANGO
Assistant Professor of Mechanical Engineering
Marquette University
Milwaukee, Wisconsin

S. M. HEINRICH
Assistant Professor of Civil Engineering
Marquette University
Milwaukee, Wisconsin

abstract

An analytical procedure evaluates contact zone characteristics and stiffness properties of circular filamentary brushes. On the basis of a large displacement mechanics analysis, filament force is evaluated for quasi-static brush contact with a flat plate. Brush stiffness properties are obtained by superimposing individual filament contact forces. Numerical examples are presented which examine contact zone characteristics and brush stiffness properties for a range of filament-work-part friction coefficients.

conference

DEBURRING AND SURFACE CONDITIONING '89
February 13-16, 1989
San Diego, California

index terms

Deburring
Mathematical Models
Metal Finishing
Tooling

1989

Society of Manufacturing Engineers • One SME Drive • P.O. Box 930
Dearborn, Michigan 48121 • Phone (313) 271-1500

ABSTRACT

In this paper, an analytical procedure is outlined which can be used for evaluating contact zone characteristics and stiffness properties of circular filamentary brushes. On the basis of a large displacement mechanics analysis, filament force is evaluated for quasi-static brush contact with a flat plate. Brush stiffness properties are obtained by superimposing individual filament contact forces. Numerical examples are presented which examine contact zone characteristics and brush stiffness properties for a range of filament-workpart friction coefficients.

1. INTRODUCTION

The use of computer-aided manufacturing methods has proven to be effective for reducing machining costs and for improving product quality and consistency of performance. However, primary machining operations such as drilling, milling, and turning can produce burrs, sharp corners or an undesirable finish. Such surface anomalies can lead to component assembly problems and unacceptable part performance or appearance. Thus, deburring and polishing operations are often necessary and may require the use of special tools for removing small amounts of material from workpart corners and edges as well as extensive surface areas. Although a variety of

deburring and surface finishing techniques have been developed, manual methods are frequently employed which utilize both rigid and compliant tools such as abrasive grinding wheels, files, coated-abrasive belts, brushes and cloth buffing wheels. Such methods are laborious, and can account for up to 35 percent of the final cost of the part. Furthermore, manual methods of deburring and surface finishing can yield widely varying quality of the final part and thus, may result in rejection of the part or contribute to reduced product performance. Automated burr removal and polishing is, therefore, an attractive alternative for reducing the cost of manufacture and increasing overall quality of the product.

In recent years, robotic methods have been developed which employ brushing tools for automated deburring and surface finishing processes. Thus, it is essential that a clear understanding of brush properties and performance characteristics be developed in order to ensure their accurate and efficient use, since the stiffness properties of brushing tools play a crucial role in assessing the dynamic response and stability of a robotic system. Furthermore, the material removal rate and surface finish quality of a workpart is closely related to the brush forces which are developed during burr removal and polishing applications. Limited technical information is available in the literature concerning the stiffness properties and machining forces of brushing tools. Recent analytical studies have been performed by the authors[1] which examine wire filament forces and brush stiffness properties for contact with a flat, frictionless surface. However, filament friction forces play a crucial role in the stiffness response and material removal process and, therefore, must be included for an improved prediction of brushing tool performance.

In this paper, a mechanics-based procedure is developed for examining the role which friction plays in the contact zone charateristics and stiffness properties of circular brushes. Coulomb friction is assumed at the interface of the filament tip and workpart surface and, on the basis of a large displacement mechanics analysis, filament force and deformation is examined. Brush stiffness is reported for quasi-static filament contact with a flat workpart.

2. MECHANICS ANALYSIS OF CIRCULAR BRUSHES

The geometry of an idealized circular brush prior to deformation is illustrated in Figure 1. All filaments are initially straight and of equal length ℓ. Each filament is assumed to be clamp-supported at the hub circumference and is aligned along the radial direction.

Geometry of a single filament in contact with a flat rigid workpart is depicted in Figure 2. The filament angle Ω defines the wire orientation at the hub. In particular, the position of the filament at initial contact with the workpart is defined by the *contact angle* Ω_C, and is related to the brush penetration depth Δ, hub radius r_h, and filament length ℓ through the following geometric relationship:

$$\Omega_C = -\cos^{-1}\left(1 - \frac{\Delta}{r_h + \ell}\right). \tag{1}$$

In addition, the *release angle* Ω_R corresponds to the filament configuration immediately before

the filament tip is released from the workpart surface S. The linear coordinate ξ is measured from the point of initial filament-workpart contact, and locates the filament tip throughout the duration of contact such that $0 \leq \xi \leq \xi_R$, where ξ_R is the length of the *contact zone*.

The configuration of a single deformed filament is illustrated in Figure 3, along with the normal and tangential components of the resultant reaction force F_{res} exerted by the workpart on the filament tip. The friction force f is assumed to be related to the normal force F through Coulomb's law:

$$f = \mu F, \tag{2}$$

where μ is the coefficient of kinetic friction. Also shown in Figure 3 is the undeformed configuration of the filament along with the component forces F_x, F_y and resultant force F_{res} which, when applied to the filament tip, result in the appropriate displacement on S. One may readily show that the following relationships are valid:

$$F_x = F_{res} cos(\alpha - \Omega), \tag{3}$$

$$F_y = F_{res} sin(\alpha - \Omega), \tag{4}$$

$$F_{res} = \frac{F}{cos(\alpha)}, \tag{5}$$

with

$$\alpha = tan^{-1}(\mu) \tag{6}$$

where α is the *friction angle*.

A geometric relationship for the displacement of the filament tip on S is readily obtained by assuming the following general representation for the deformed filament:

$$v = v(u), \tag{7}$$

where v is the transverse displacement in the y-direction, and u is the x-coordinate of the section of interest *after* deformation. Thus, if $u = u^*$ corresponds to the coordinate of the filament tip, then the displacement of the tip is $v^* = v(u^*)$. Since the filament tip must lie on S, one may show that the following geometric constraints must be satisfied:

$$u^* = (r_h + t)cos(\Omega - \Omega_C) + \xi sin(\Omega) - r_h, \tag{8}$$

$$v^* = (r_h + t)sin(\Omega - \Omega_C) - \xi cos(\Omega). \tag{9}$$

Assuming that axial deformation of the filament is negligible, a third geometric constraint may be obtained in integral form:

$$\int_0^{u^*} \sqrt{1 + [v'(u)]^2}\, du = t. \tag{10}$$

The slope of a deformed filament may become large during brushing processes and, therefore, it is necessary to use the exact expression for the bending moment-curvature relationship of an elastic filament [2]:

$$\frac{M(u)}{EI} = \frac{v''(u)}{\{1 + [v'(u)]^2\}^{3/2}} \tag{11}$$

where

$$M(u) = (u^* - u)F_y + [v(u^*) - v(u)]F_x \tag{12}$$

is the bending moment at section u, and primes ($'$, $''$) denote differentiation with respect to u. Thus, by utilizing Eqs. (3), (4), (5) and (6) in conjunction with Eqs. (11) and (12), the governing equation for bending of a single filament may be written as

$$v''(u) = \frac{F}{EI}\sqrt{1+\mu^2}\{1 + [v'(u)]^2\}^{3/2}\{sin(\alpha - \Omega)(u^* - u) + cos(\alpha - \Omega)[v(u^*) - v(u)]\}. \tag{13}$$

Boundary conditions at the hub are given by

$$v(0) = 0, \tag{14}$$

$$v'(0) = 0, \tag{15}$$

while the condition of zero moment at the filament tip dictates that

$$v''(u^*) = 0. \tag{16}$$

Equation (13), boundary conditions (14), (15), and (16), and the geometric constraints (8), (9), and (10) comprise the mathematical formulation for constrained deformation of a single filament in contact with the workpart. Thus, for specified values of t, r_h, Δ, μ, Ω, and EI, the parameters to be determined are $v(u)$, u^*, ξ, and F. In the next section a systematic procedure will be summarized for obtaining a numerical solution to the problem.

It is interesting to note that the form of the above mathematical model indicates that a change in the filament flexural rigidity EI will only alter the solution by changing the normal force in direct proportion; that is

$$\frac{F}{EI} = constant. \tag{17}$$

for *any* choice of EI. Thus, if a normal force F_1 corresponding to flexural rigidity $(EI)_1$ has been determined, then the normal reaction associated with $(EI)_2$ can immediately be obtained from

$$F_2 = \frac{(EI)_2}{(EI)_1}F_1. \tag{18}$$

The deformed filament shape, or *elastica*, will not be influenced by the change in EI.

Upon obtaining a solution for the constrained deformation of a single filament, one may evaluate the overall properties of a circular brush by appropriately superimposing the contribution of each filament in contact with S. For example, the service torque $\mathcal{T}$ (per plane of filaments) required to keep the brush in equilibrium at a penetration depth Δ, is given by

$$\mathcal{T} = \sum_{i=1}^{N_S} T_i, \tag{19}$$

where N_S is the number of filaments in contact with S, and

$$T_i = (r_h + t + \Delta) f_i - [(r_h + t)sin(\Omega_C) + \xi_i] F_i \tag{20}$$

is the torque associated with the i^{th} filament. Similarly, the magnitude of the resultant force between the brush and workpart for a single plane of filaments may be obtained from

$$\mathcal{F} = \frac{1}{cos(\alpha)} \sum_{i=1}^{N_S} F_i. \tag{21}$$

The resultant brush stiffness K is defined as the local slope, or *tangent stiffness*, of the $\mathcal{F}$-Δ response curve:

$$K = \frac{d\mathcal{F}}{d\Delta}. \tag{22}$$

The corresponding normal and shear stiffnesses of a brush, per plane of filaments, are given by

$$K_n = K cos(\alpha), \tag{23}$$

and

$$K_s = K sin(\alpha), \tag{24}$$

respectively. Overall brush stiffness may be obtained by summing the contribution of all planar sections of filaments for a particular brush system. Thus, the overall resultant brush stiffness is

$$\mathcal{K} = nK, \tag{25}$$

where n is the number of planar sections occupied by filaments, as shown in Figure 1.

As noted previously, the relationship $\frac{F}{EI} = constant$ is valid for any choice of flexural rigidity EI. Thus, numerical results for force, torque, and stiffness will be reported in the more useful reduced forms $\frac{\mathcal{F}}{EI}$, $\frac{\mathcal{T}}{EI}$, and $\frac{K}{EI}$.

3. SOLUTION METHOD FOR EVALUATING CONSTRAINED FILAMENT DEFORMATION

In this section, the numerical method used for obtaining solutions for constrained filament deformation is briefly outlined. By employing a standard reduction of order technique[3], Eq. (13) is rewritten

$$g_1'(u) = g_2(u) \tag{26}$$

$$g_2'(u) = -\frac{F}{EI}\sqrt{1+\mu^2}[1+g_2^2(u)]^{\frac{3}{2}}\left[sin(\Omega)(u^* - u) - cos(\Omega)(v^* - g_1(u))\right] \tag{27}$$

along with the initial conditions

$$g_1(0) = 0 \tag{28}$$

$$g_2(0) = 0 \tag{29}$$

where the change of variables $g_1(u) = v(u)$ and $g_2(u) = v'(u)$ has been employed.

The solution procedure used in the present research employs an iterative approach for obtaining F and Ω which, in addition to satisfying Eqs. (26)-(29), also minimizes

$$\Psi_1 = |v^* - g_1(u^*)| \tag{30}$$

$$\Psi_2 = |t - \int_0^{u^*} \sqrt{1+g_2^2(u)}\, du|. \tag{31}$$

Thus, Eqs. (26)-(31) comprise the system of differential equations along with the appropriate boundary conditions and constraints which, when satisfied, yield solutions for quasi-static filament-workpart contact. Addition details concerning the procedure used for obtaining numerical solutions for (u, v) along equispaced $\xi^{(k)}$, $(k = 1, 2, ...)$ can be found in Ref. 1.

4. RESULTS AND DISCUSSION

In this section, numerical results are reported for filament contact zone characteristics and brush stiffness properties for a range of penetration depths and friction conditions. For illustrative purposes, the overall brush diameter $D = 15.24\ cm$ $(6.0\ in.)$, brush geometry $t/r_h = 1.0$, and number of planar filaments $N = 500$, are used throughout the numerical studies. Numerical solutions are obtained which satisfy Eqs. (26) and (27), along with the conditions (28)-(31). The filament-release mechanics for friction-free contact with a flat plate has been discussed by the authors in an earlier paper[1]. The release angle Ω_R reported in the current research is taken as the largest value of Ω for which a numerical solution can be obtained.

In Figure 4, the magnitude of the resultant filament force F_{res}/EI along the workpart coordinate ξ is illustrated for penetration depth $\Delta = 0.254\ cm$ $(0.1\ in.)$. Frictionless filament contact yields a large resultant force and resultant force gradient near the release position, ξ_R. However, filament contact forces undergo a rapid decline as the frictional coefficient is increased from $\mu = 0.0$ to $\mu = 1.5$.

The effect of friction on the distribution of filaments $P = (1 - N_\xi/N_S)$, along the normalized contact zone $\hat{\xi} = \xi/\xi_R$ is shown in Figure 5 for a brush having $N = 500$ equispaced filaments, subjected to penetration depth $\Delta = 0.254\ cm$ $(0.1\ in.)$. The nomenclature N_ξ and N_S refer to the numbers of filaments on S over the partial region $0 \leq \bar{\xi} \leq \xi$ and the total contact zone ξ_R, respectively. It is observed that workpart friction has a negligible effect on the filament population distribution along the workpart. That is, for the range of frictional conditions examined, a sparse number of filaments are located near the release position $\hat{\xi} \approx 1$, while a large percentage of filaments occupy the initial contact region $\hat{\xi} \approx 0$.

In Figure 6, the relationship between contact zone size ξ_R and penetration depth Δ is examined. The size of the contact zone is virtually unaffected for the range of friction coefficients $\mu = 0.3$ to $\mu = 1.5$. However, an abrupt increase of the contact zone size (approximately thirteen percent) is noted when comparison is made between the results reported for $\mu = 0$ and $\mu \neq 0$.

Resultant brush force $\mathcal{F}/EI$ for various brush penetration depths Δ and friction coefficients μ is illustrated in Figure 7, whereby it is noted that an increase of filament-workpart friction leads to a consecutive reduction of the resultant brush force. Furthermore, it is observed that for all frictional conditions reported, an essentially linear relationship between $\mathcal{F}/EI$ and Δ is obtained for $\Delta > 0.2\ cm$ $(0.079in.)$.

In Figure 8, the relationship between applied brush torque $\mathcal{T}/EI$ and brush penetration depth Δ is examined for a range of frictional coefficients. In each case, an increase of friction coefficient yields an increased brushing torque for the quasi-static service load. Furthermore, an approximately linear relationship between $\mathcal{T}/EI$ and Δ is obtained for the range of friction coefficients and brush penetration depths reported.

The brush stiffness properties which were evaluated on the basis of Eq. (22) along with the data appearing in Figure 7, are shown in Figure 9 for various frictional conditions. An apparent reduction of brush stiffness is obtained as the filament-workpart friction coefficient is successively increased. However, the stiffness reduction is greatest at small penetration depths $(\Delta \leq 0.2\ cm\ (0.079in.))$, and least at large penetration depths. It is interesting to note that, at the greatest penetration depth examined $(\Delta = 0.762\ cm\ (0.3\ in.))$, the brush stiffness properties are approximately uniform for all friction conditions examined. This observation is consistent with the similar slopes that are reported in Figure 7 at the greatest penetration depth.

Brush force and stiffness component data can provide engineers with important information concerning the anticipated performance of brushing tools during polishing and deburring applications. Thus, the brush stiffness reported in Figure 9 for $\mu = 0.6$ is repeated in Figure 10, along with the associated normal and shear stiffness component properties K_n and K_s, respectively.

5. SUMMARY AND CONCLUSIONS

The effect of workpart-filament friction on brush performance properties has been investi-

gated by means of a quasi-static large deformation elastic analysis. A mechanics-based formulation has been employed in conjunction with a systematic numerical procedure to solve the problem of constrained deformation of a single filament. Overall brush properties were subsequently obtained by superimposing the forces associated with a distribution of filaments located along the workpart surface. Force and torque quantities were reported to be proportional to the flexural rigidity, EI; therefore, these data have been reported in reduced form (scaled by EI) in order to render the numerical results applicable for a range of filamentary materials and cross-section shapes. Additional theoretical considerations are currently being examined by the authors, including the effect of workpart geometry on brush stiffness response and contact zone characteristics. Other aspects of the problem which merit attention include the evaluation of brush width distortion during brushing processes, and the assessment of dynamic brush properties associated with steady rotation of the brush.

6. ACKNOWLEDGMENTS

The authors gratefully acknowledge contributions made by Dr. Nicholas Nigro, Professor of Mechanical Engineering at Marquette University. This research was sponsored in part by the Milwaukee Brush Manufacturing Company under M.U. Grant 5966. Valuable discussion with Mr. James Henderson, Director of Engineering at the Milwaukee Brush Mfg. Co., is gratefully acknowledged.

7. REFERENCES

[1] Stango, R. J., Heinrich, S. M., and Shia, C. Y., "Analysis of Constrained Filament Deformation and Stiffness Properties of Brushes", *ASME Proceedings, Computer-Aided Design and Manufacture of Dies and Molds*, Winter Annual Meeting, 1988, Chicago, IL. Production Engineering Division, Vol. 32, pp. 91–103.

[2] Gere, J. M., and Timoshenko, S. P., *Mechanics of Materials*, Second Edition, 1984, Wadsworth, Inc., Belmont, CA, pp. 351–355, 414–415.

[3] Hamming, R. W., *Numerical Methods for Scientists and Engineers*, 1973, McGraw-Hill, Inc., NewYork, NY, pp. 391–392.

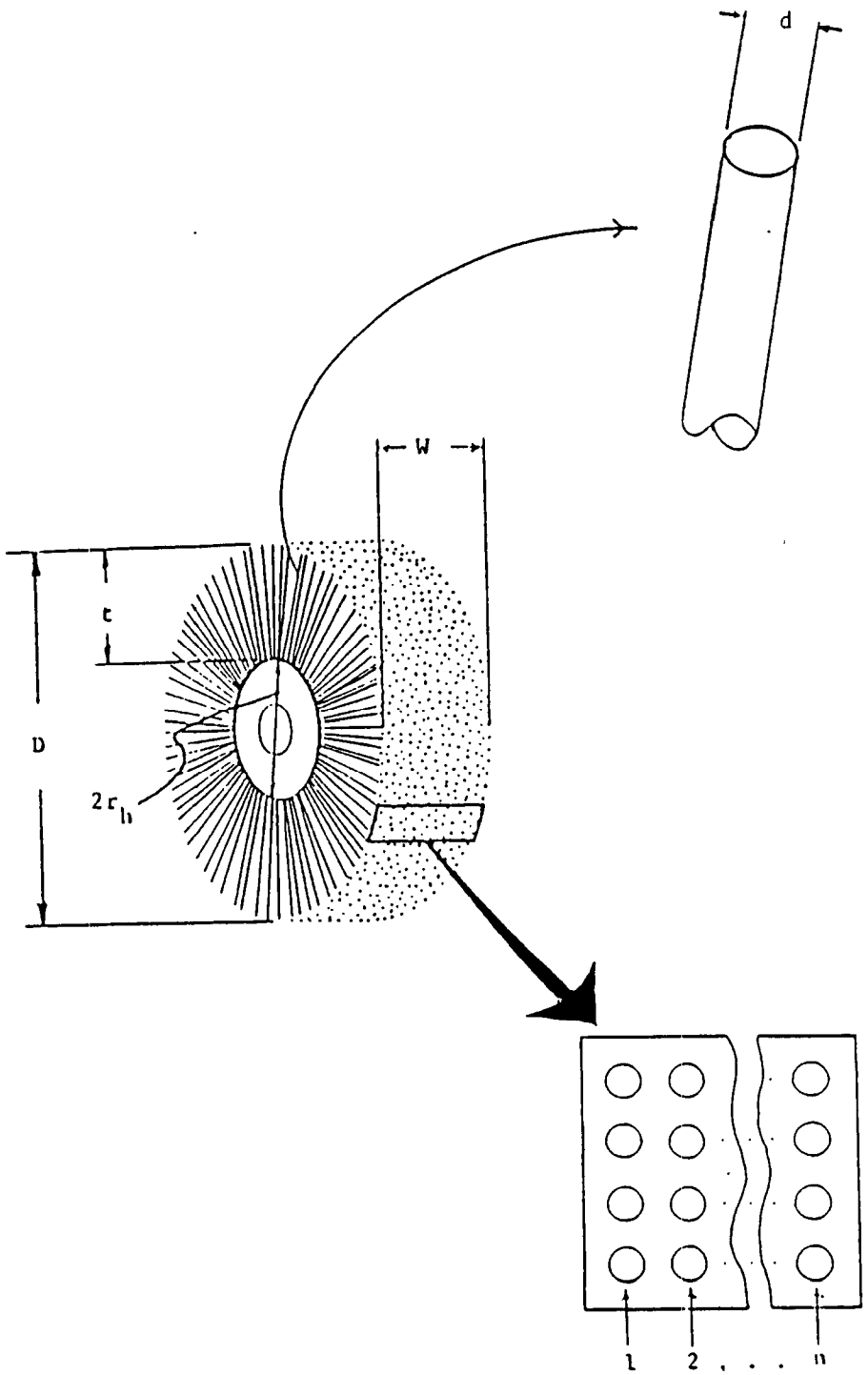

Fig. 1. Geometry of a Circular Filamentary Brush

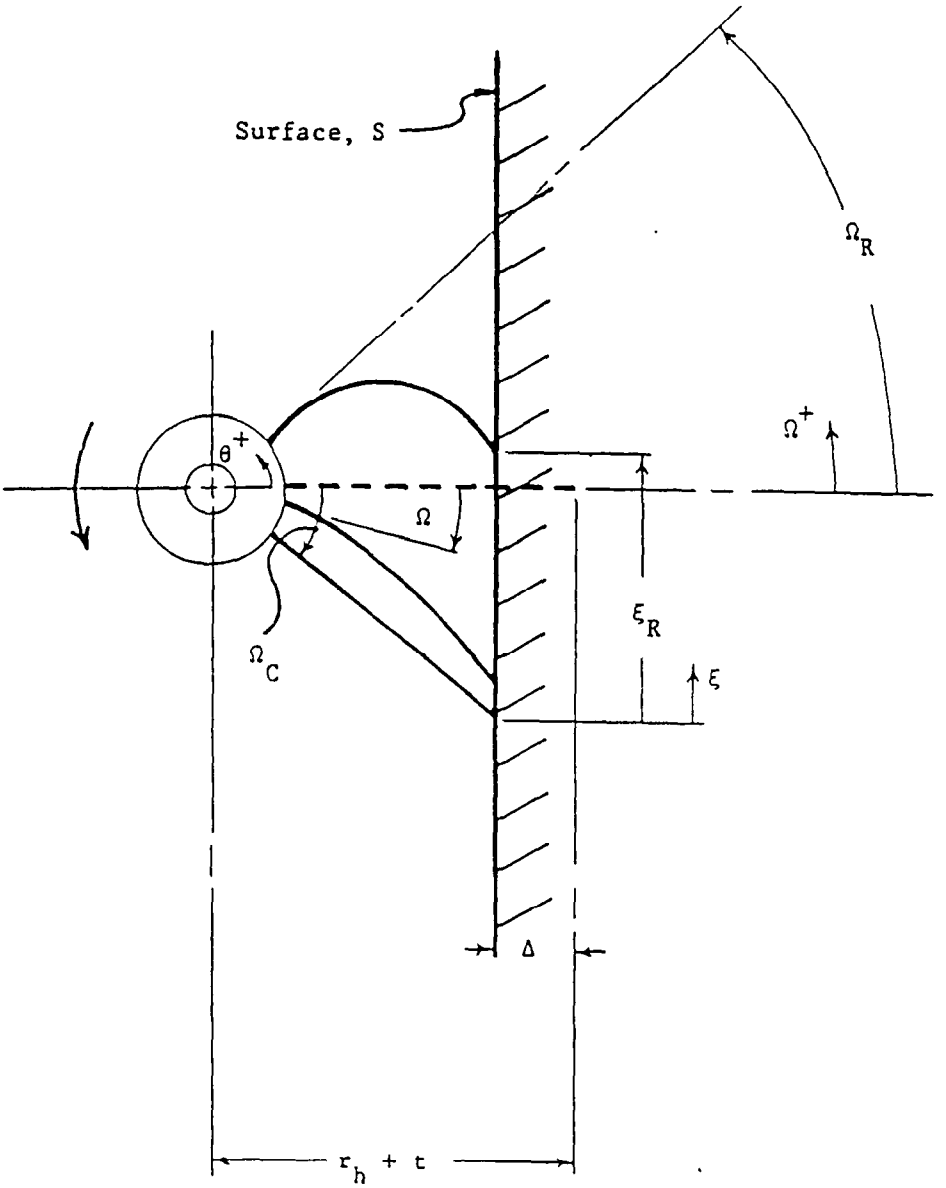

Fig. 2. Deformation of a Single Filament at the Initial, Intermediate and Release Positions

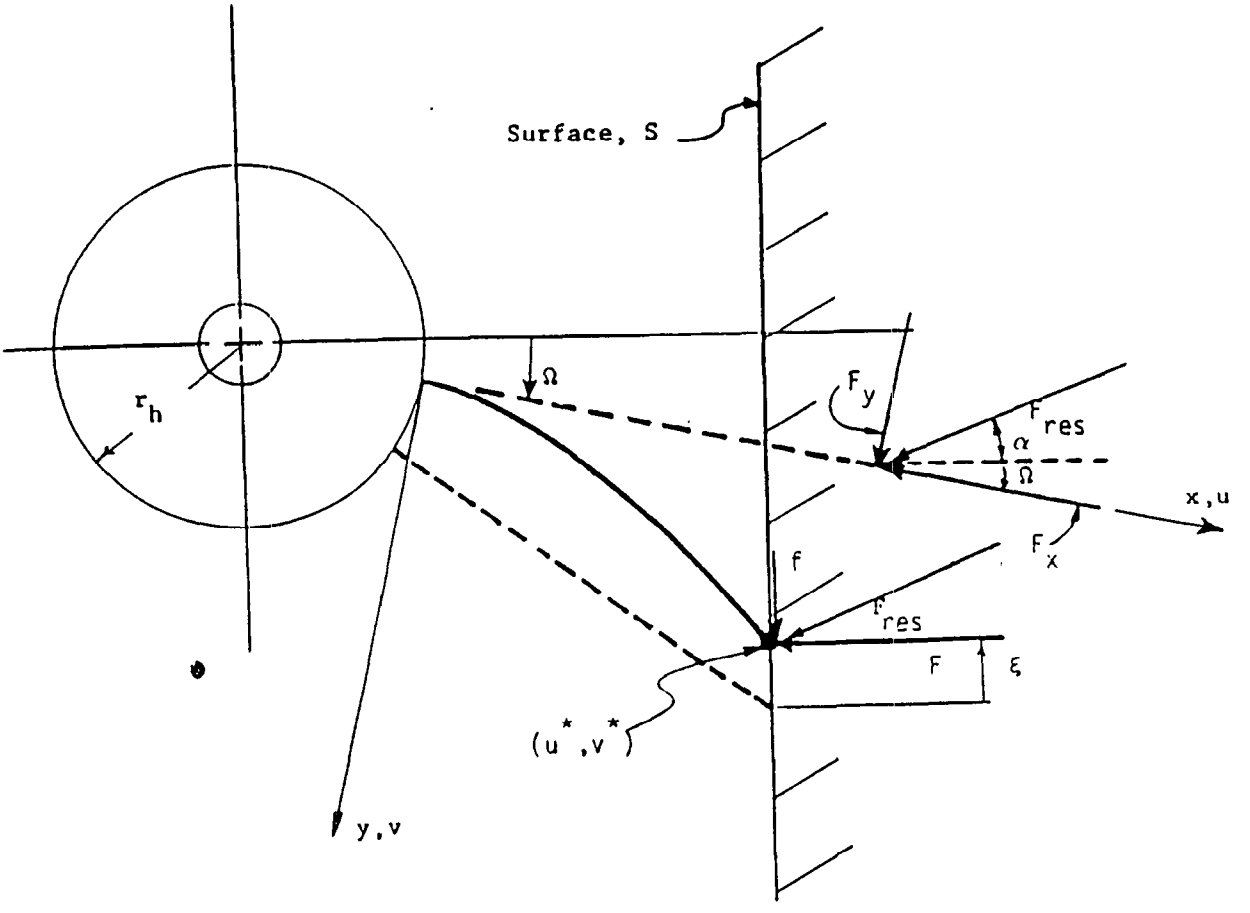

Fig. 3. Deflection of Filament and Corresponding Filament Load for the Initial and Deformed Configurations

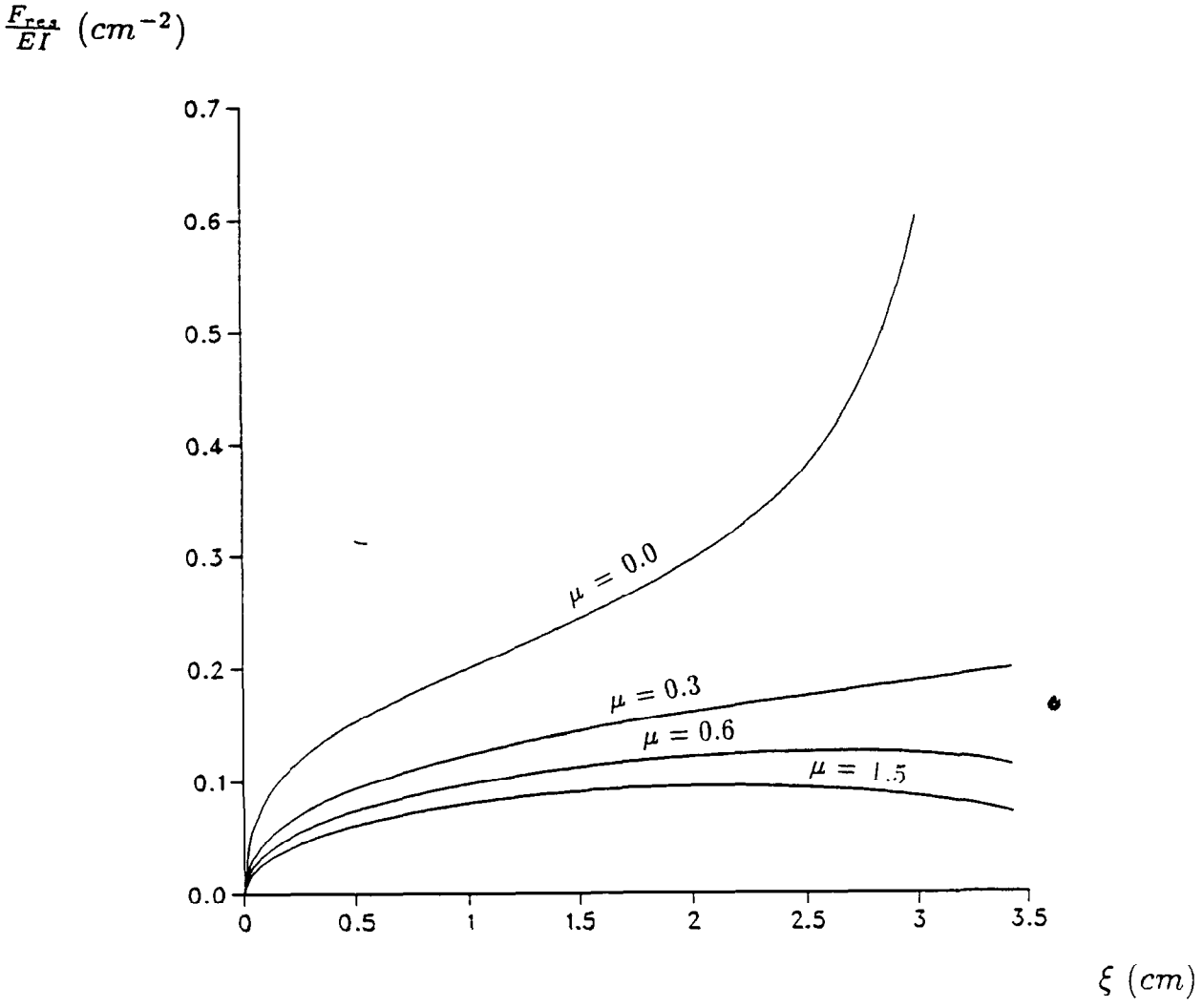

Fig. 1. Filament Force F_{res}/EI Along ξ Coordinate for $\mu = 0.0$, 0.3, 0.6 and 1.5

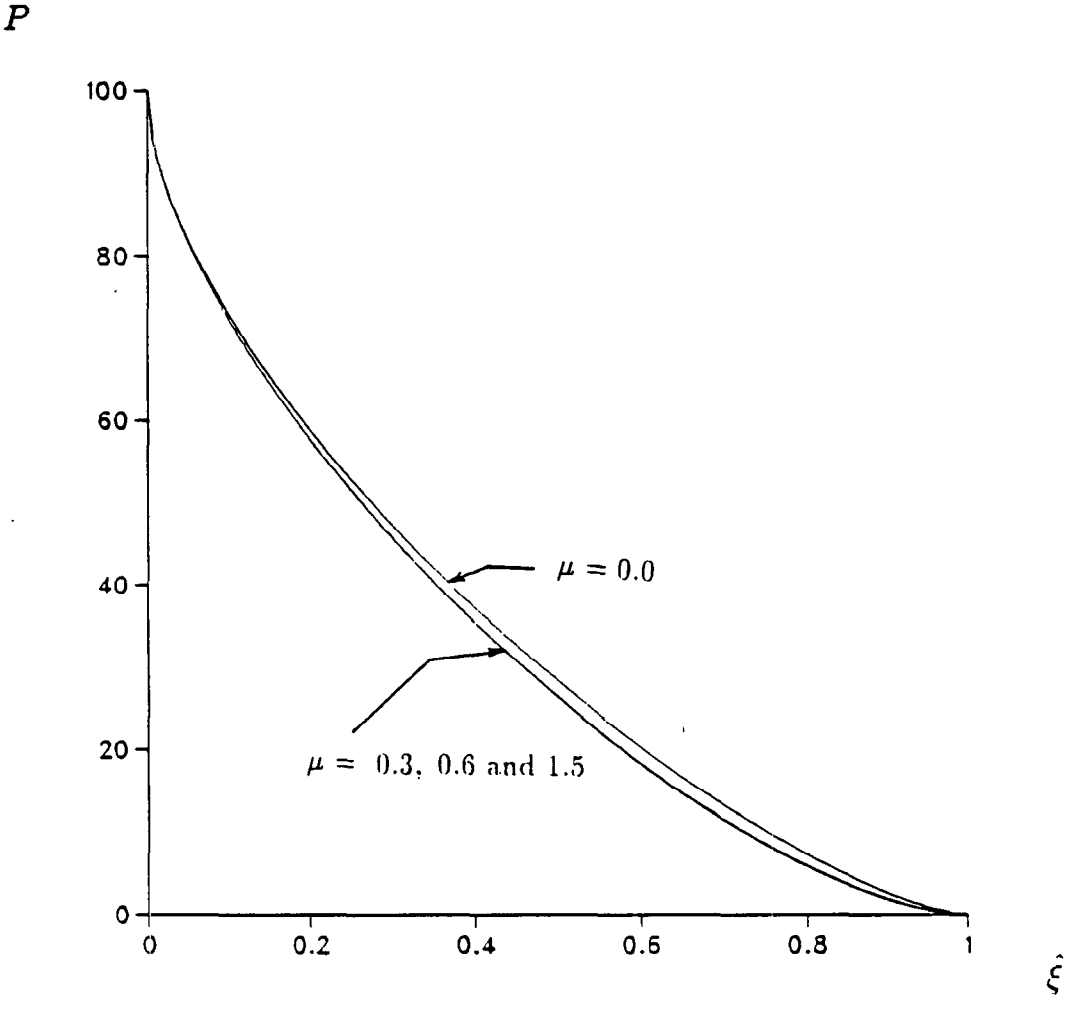

Fig. 5. Percentage P of All Filaments in the Contact Region, Located within the Subregion $\hat{\xi} \leq \bar{\xi} \leq 1$, for $\mu = 0.0$, 0.3, 0.6 and 1.5

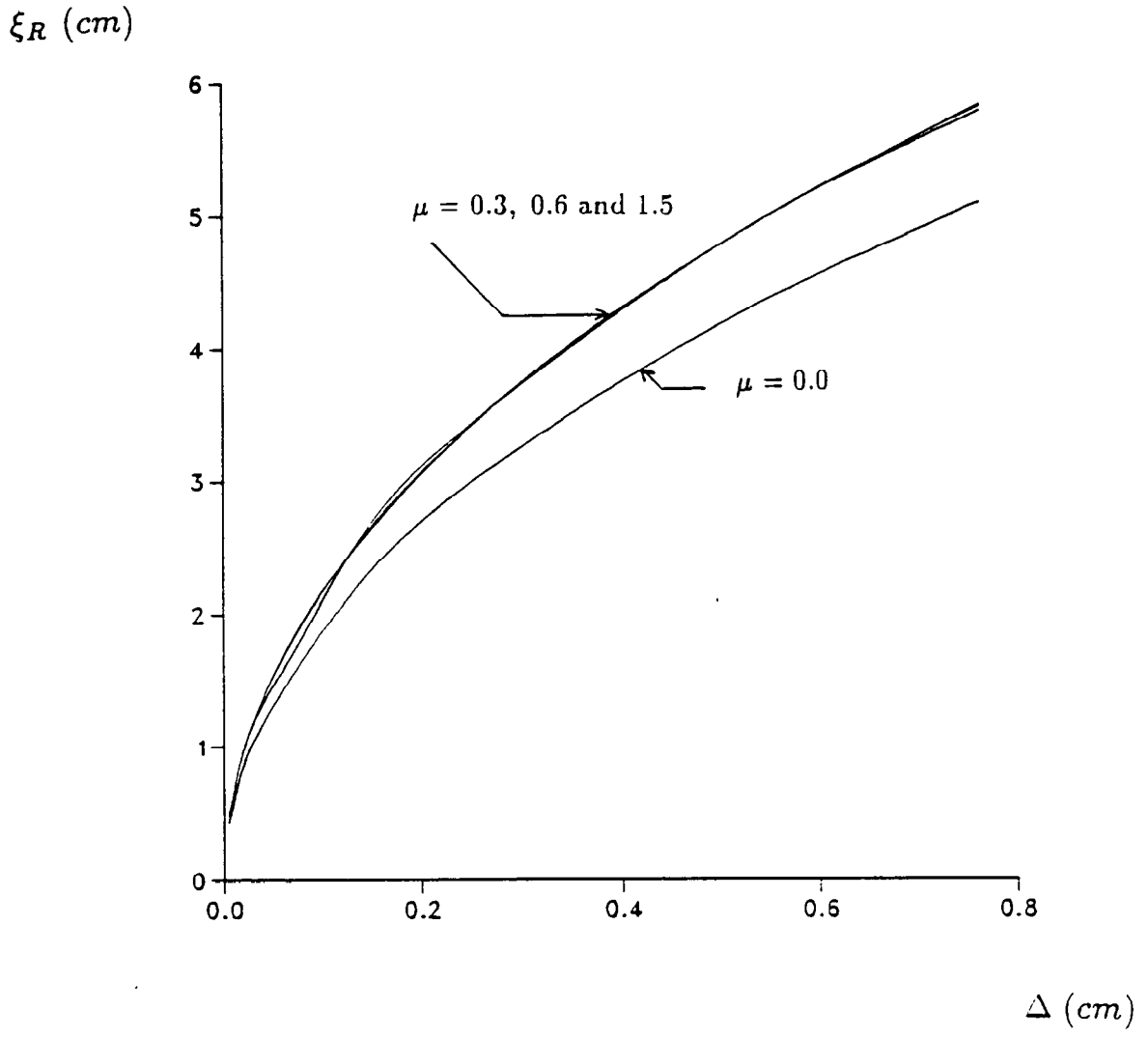

Fig. 6. Length of Filament Contact Zone ξ_R vs. Brush Penetration Depth Δ for μ = 0.0, 0.3, 0.6 and 1.5

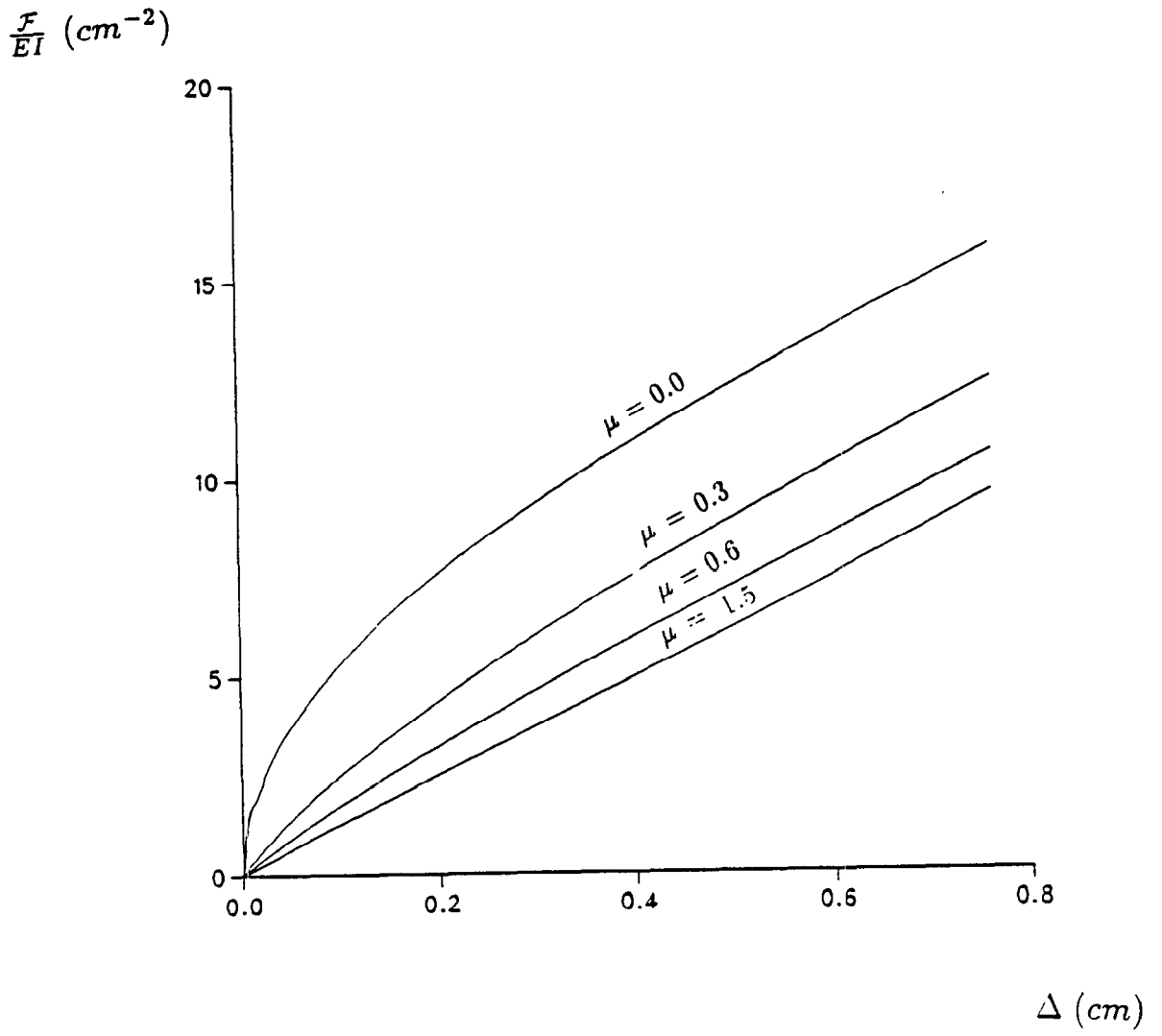

Fig. 7. Brush Resultant Force $\frac{\mathcal{F}}{EI}$ vs. Brush Penetration Depth Δ for $\mu = 0.0$, 0.3, 0.6 and 1.5

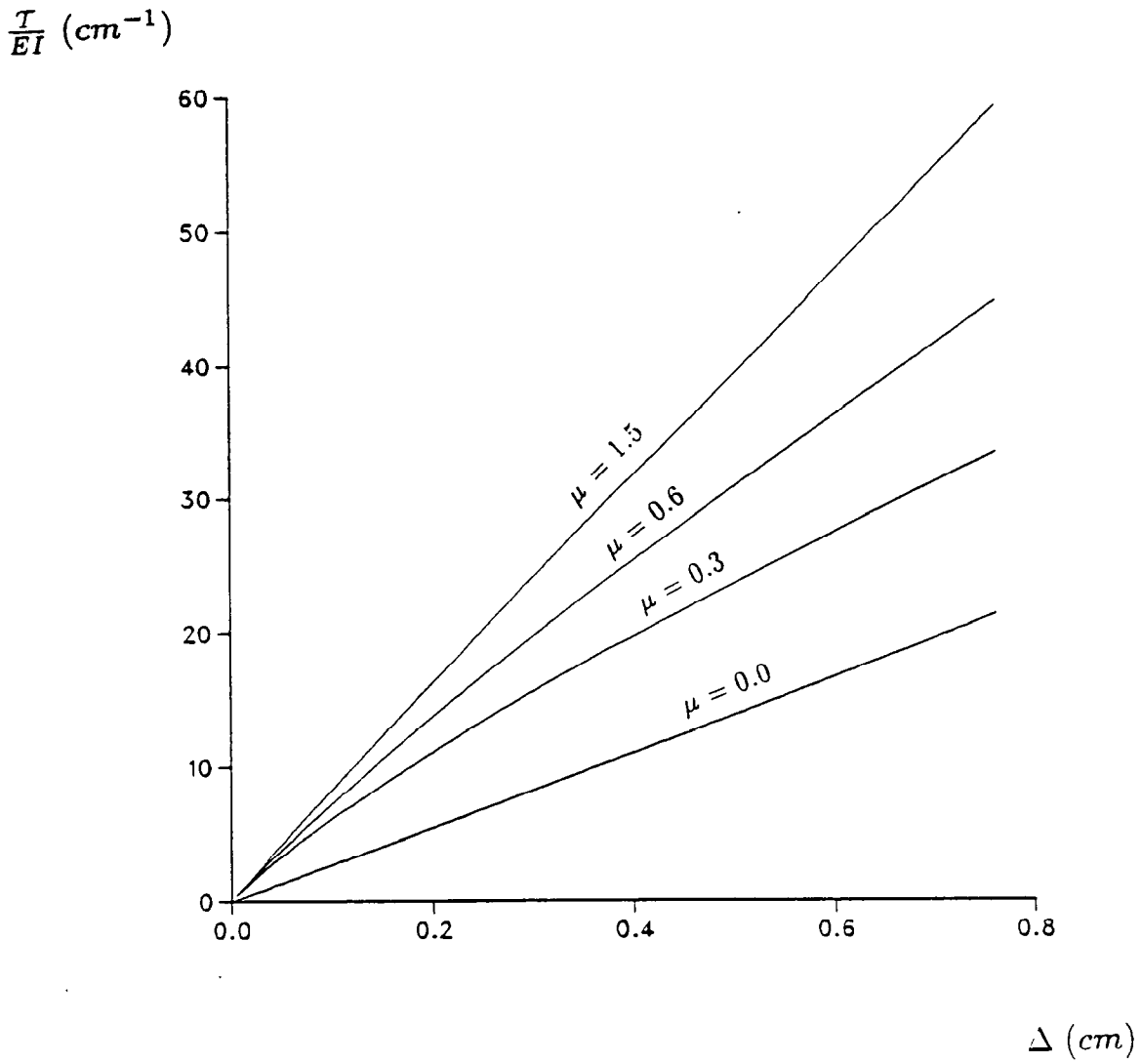

Fig. 8. Brush Resultant Torque $\frac{\mathcal{T}}{EI}$ vs. Brush Penetration Depth Δ for $\mu = 0.0$, 0.3, 0.6 and 1.5

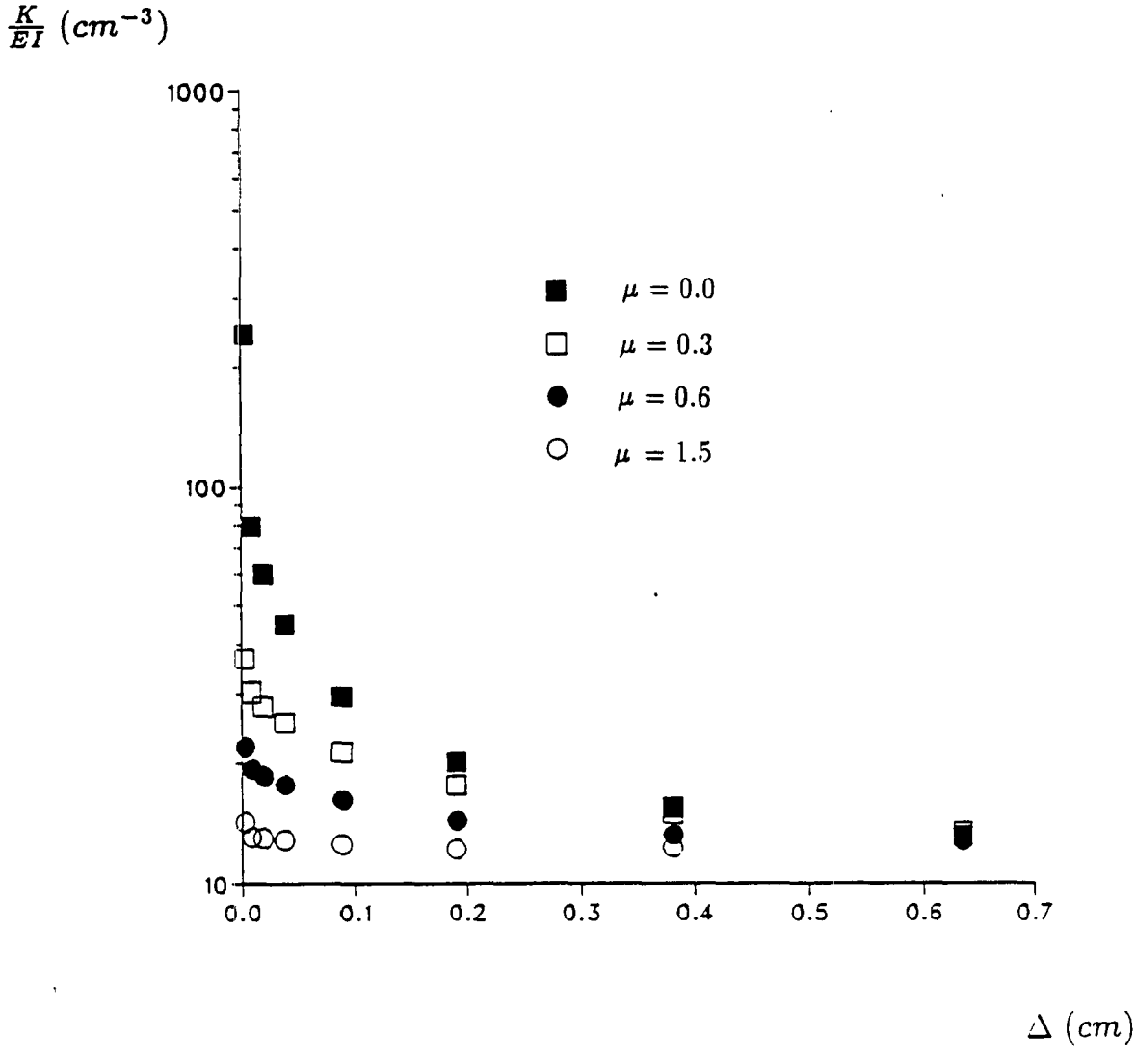

Fig. 9. Brush Stiffness $\frac{K}{EI}$ vs. Brush Penetration Depth Δ for $\mu = 0.0$, 0.3, 0.6 and 1.5

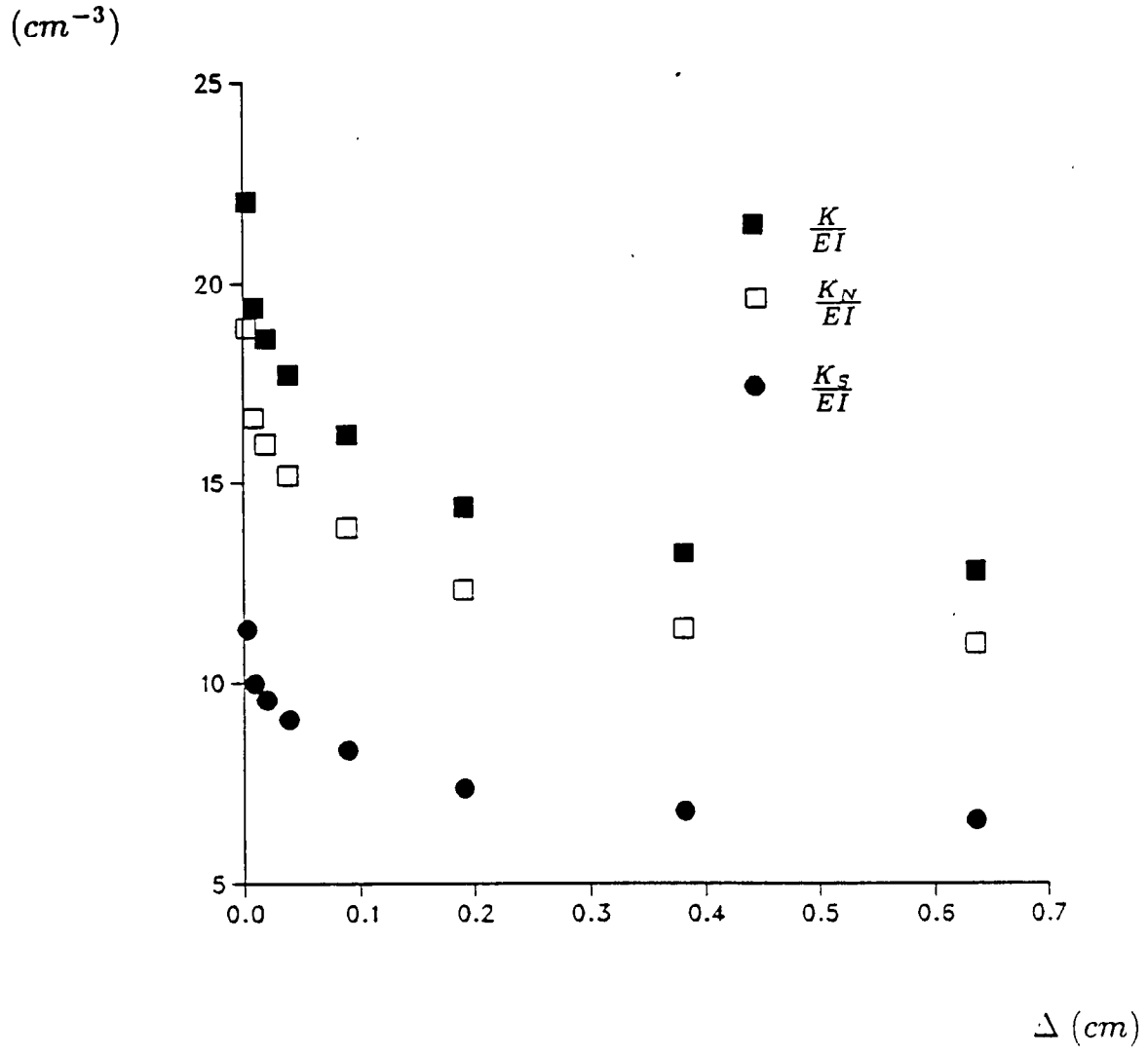

Fig. 10. Normal, Shear and Resultant Brush Stiffness vs. Brush Penetration Depth Δ for $\mu = 0.6$